Spectrochimica Acta Part A: Molecular and Biomolecular Spectroscopy 216 (2019) 154–160

Contents lists available at ScienceDirect

Spectrochimica Acta Part A: Molecular and Biomolecular Spectroscopy

journal homepage: www.elsevier.com/locate/saa

Simultaneous multi-gas detection between 3 and 4 μm based on a 2.5-m multipass cell and a tunable Fabry-Pérot filter detector

Shangzhi Li [a,b], Lei Dong [a,b,*], Hongpeng Wu [a,b], Xukun Yin [a,b,d], Weiguang Ma [a,b], Lei Zhang [a,b], Wangbao Yin [a,b], Angelo Sampaolo [a,c], Pietro Patimisco [a,c], Vincenzo Spagnolo [a,c,**], Suotang Jia [a,b], Frank K. Tittel [d]

[a] State Key Laboratory of Quantum Optics and Quantum Optics Devices, Institute of Laser Spectroscopy, Shanxi University, Taiyuan 030006, China
[b] Collaborative Innovation Center of Extreme Optics, Shanxi University, Taiyuan 030006, China
[c] PolySense Lab, Physics Department, Politecnico di Bari, Bari I-70100, Italy
[d] Department of Electrical and Computer Engineering, Rice University, Houston, TX 77005, USA

ARTICLE INFO

Article history:
Received 31 January 2019
Received in revised form 4 March 2019
Accepted 10 March 2019
Available online 11 March 2019

Keywords:
Optical gas sensor
Fabry-Pérot filter detector
Multi-gas detection

ABSTRACT

We demonstrated a versatile and innovative gas sensing system based on a Fabry-Pérot (FP) filter detector, which operates in the spectral range from 3.1 to 4.4 μm (3226–2273 cm^{-1}) with a spectral resolution of 20 nm. The developed sensor system can be used to record the entire spectrum by means of a one-time scan or, alternatively, to access selected spectral regions by using the tunable FP filter detector. A multipass cell with an effective path length of 2.5 m was implemented to improve the detection sensitivity. The spectra of methane, formaldehyde and carbon dioxide were simultaneously measured, with detection limits of 200 ppm, 900 ppm and 20 ppm, respectively. A seven-day continuous measurement for indoor carbon dioxide gas was carried out demonstrating the stability and robustness of the reported sensor system.

1. Introduction

Absorption spectroscopy in the mid-infrared (mid-IR) spectral range is a versatile detection technique for identifying the composition of gas mixtures and determining their concentration levels, since the strongest absorbing features of many highly targeted and important molecules are located in this range [1–3]. The 3–4 μm spectral window is the finger print region of many important hydrocarbons, such as methane (CH_4), ethane (C_2H_6), propane (C_3H_8), ethylene (C_2H_4), propylene (C_3H_6) and acetylene (C_2H_2), and some of them characterized by broadband absorption profiles [3,4]. Formaldehyde (CH_2O), widely used in industrial manufacturing of products, and carbon dioxide (CO_2) also have strong absorption features located in this spectral window [5–7]. Hence, there is a growing demand for robust, cost-effective, multi-gas sensor systems operating in the 3–4 μm spectral range, capable to perform environmental monitoring, chemical analysis, industrial process control, medical diagnosis and pollution monitoring.

To target these applications, many optical detection techniques were optimized and adopted [8–24]. Conventional Fourier transform infrared (FTIR) spectroscopy present, so far, the most flexible technique, capable to cover from near to far infrared spectral ranges [25–29]. The filter-based mid-IR gas detection technique is a low-cost alternative method that relies on the employment of an incoherent light source for detecting broadband absorbers [30–32]. A filter-based gas sensor usually employs an IR detector with spectrally selective filters, each of them allows to access to a small fixed range of the IR spectrum. As a result, such a detector exhibits high selectivity in an open-air condition. Although the spectral coverage and resolution cannot compete with expensive FTIR-based spectrometers, low-cost filter-based gas sensors offer adequate performance making them attractive and suitable for multi-gas environmental detection, when detection limits in the ppm range are required [33,34].

Multi-gas detection based on a filter-based gas sensor is usually implemented by employing a rotating filter wheel with multiple filters. However, only a limited number of filters can be mounted on a wheel and, as a result, the spectral resolution across a specific spectral region is accordingly reduced [35]. Furthermore, the spectral response of filters must exactly match the specific gas absorption band in order to meet the measurement requirements. For the detection of gas species with absorption bands spaced by few tens of cm^{-1}, there is specific requirement of the spectral specifications of narrow-band filters.

Recently, a Fabry-Pérot (FP) filter detector based on microelectromechanical systems (MEMS) has been reported [36,37]. The detector integrates a FP interferometer and a pyroelectric detector

* Correspondence to: L. Dong, State Key Laboratory of Quantum Optics and Quantum Optics Devices, Institute of Laser Spectroscopy, Shanxi University, Taiyuan 030006, China.
** Correspondence to: V. Spagnolo, PolySense Lab, Physics Department, Politecnico di Bari, Bari I-70100, Italy.
E-mail addresses: donglei@sxu.edu.cn (L. Dong), vincenzoluigi.spagnolo@poliba.it (V. Spagnolo).

https://doi.org/10.1016/j.saa.2019.03.025
1386-1425/

into a compact TO8 housing equipped with a signal preamplifier. The FP interferometer consists of two flat and parallel reflector plates, acting as half-wave resonator and producing a series of transmittance peaks of successive interference orders. The spacing between the two plates is varied by using a driving voltage, tuning both the peak positions and the center wavelength of the incident optical beam on the pyroelectric detector. An additional band-pass optical filter is placed in series with the FP interferometer to remove undesired harmonics. Therefore, the FP filter detector can transmit selected wavelength ranges by adjusting the driving voltage of the FP interferometer [38,39]. The MEMS based FP filter detector has a small footprint, low-cost and high ruggedness and can cover a large spectral range with a continuous wavelength tunability and without the requirements of any additional precision optics. These new designs can be mass-produced, covering different mid-IR spectral region. Therefore, the use of a tunable filter instead of a narrow-band filter can remove the restrictions imposed by rotating wheel filter-based sensors, realizing a compromise between performance and price, and paving the way to measure several gases at one time with a single detector.

To obtain a high detection sensitivity, a long effective absorption pathlength is required according to Beer-Lambert law. With a filter-based gas sensor, the short absorption path in filter-based gas sensors limits their detection sensitivity, due to the fact that it is a challenge to collimate an incoherent light beam with a large divergence angle to pass through a long pathlength.

In this paper, we describe an optical sensor for multi-gas detection based on a FP filter detector. The optical sensor employed a SiC thermal light source emitting in a broad spectral range between 1 μm and 25 μm. The absorption spectra of three species (CH_4, CH_2O and CO_2) were simultaneously measured by the FP filter-based sensor, operating in the 3–4 μm wavelength range. In order to improve the detection sensitivity, a multipass cell with an effective pathlength of 2.5 m was coupled with the FP filter detector, resulting in a sensitive and cost-effective gas sensor system.

2. Sensor design

The operating principle of the FP-based optical sensor allows arbitrary access to selected spectral regions by adjusting the MEMS control voltage. In this way, the FP filter control can be used to monitor a broad spectral region, continuously. When a specific transmitted wavelength is selected, the full widths at half maximum (FWHM) of the transmission band can be expressed by the following expression [35,40]:

$$FWHM = \frac{2d}{\pi m^2}\sqrt{\frac{(1-R)^2}{R}} \quad (1)$$

where d is the distance between the reflective surfaces, m is the interference order and R is the reflectivity. Usually, a FWHM of typically 30–70 cm^{-1} can be achieved.

For wavelength calibration, the FP filter implemented in this work (InfraTec GmbH, Model LFP-3144C-337) was coupled to a Thermo Scientific Nicolet iS50 FTIR spectrometer acting as an external detector. Transmission windows of the FP filter were measured at different driving voltages by averaging 32 scans, as shown in Fig. 1(a), corresponding to the spectral range from 3.1 to 4.4 μm (3226–2273 cm^{-1}). The transmissivity exhibits a nearly linear decrease with the increasing voltages from 25.3 V to 34.9 V and starts to rise at 35.7 V. Moreover, there is a transmissivity valley in the range of 18.8V to 25.3V. Therefore, background elimination is required for the multi-gas sensing. The FWHMs and the driving voltages as a function of wavenumber are plotted in Fig. 1(b). The FWHMs of the transmission curves increase from 30 cm^{-1} up to 65 cm^{-1} in the investigated voltage range, with the smallest value measured at 2273 cm^{-1} (17 V). The relationship

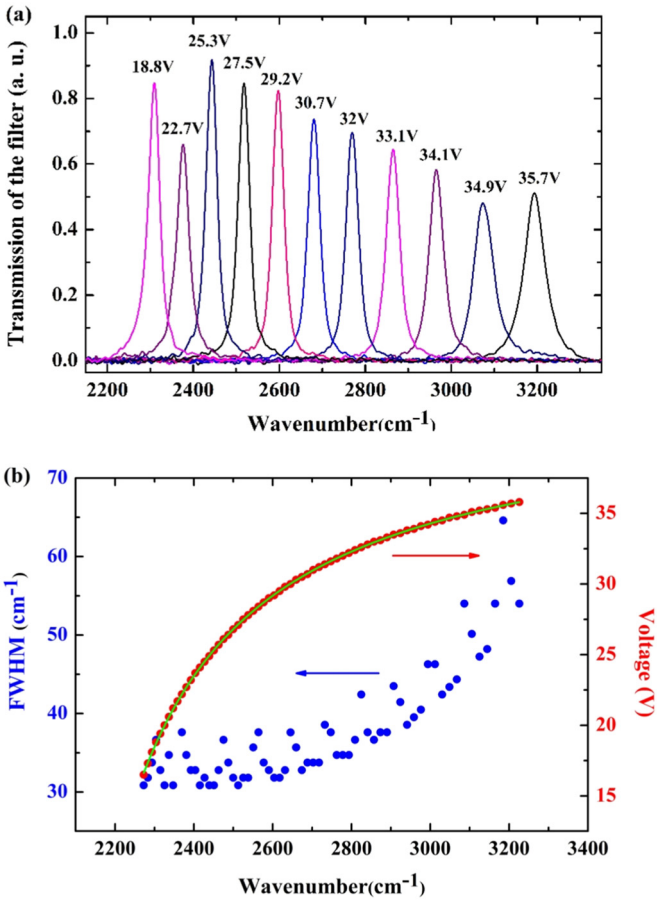

Fig. 1. (a) Transmission windows of the LFP-3144C-337 when different driving voltages are applied. (b) FWHMs (blue dots) of the transmission curves and the related applied voltage (red dots) measured as a function of wavenumber. The green solid line represents the best fit using Eq. (2). (For interpretation of the references to colour in this figure legend, the reader is referred to the web version of this article.)

between driving voltage V_d and central transmission wavenumber $\bar{\nu}$ can be expressed as [38]:

$$V_d = V_{asy} - \frac{a}{\bar{\nu} - \bar{\nu}_{asy}} \quad (2)$$

where V_{asy} and $\bar{\nu}_{asy}$ are two asymptotic values of the inverse function and a is a constant factor. Eq. (2) was fitted to the measured transmission spectra, producing a = 9647.93 $cm^{-1}V$, V_{asy} = 43.12 V and $\bar{\nu}_{asy}$ = 1 908.62 cm^{-1}, which can be used to calibrate the wavenumber axis and set the scanning with an equidistant step size.

A broadband thermal light source (Hawkeye Technologies, Model IR-Si 207) was chosen as the mid-infrared light source. Its emission spectrum, spanning from 1 μm to 25 μm, was measured by the FTIR spectrometer, as shown in Fig. 2. The emission spectrum has a strong light intensity between 2.5 and 7 μm. The inset in Fig. 2 shows the emission spectra in the tuning range of the FP filter from 3.1 to 4.4 μm. The valleys around 3.4 μm and 4.25 μm are due to the absorption of methane and carbon dioxide in air, respectively.

The multi-gas optical sensor based on a FP filter detector and a multipass gas cell is schematically depicted in Fig. 3. The optical sensor system, which has dimensions of 40 × 20 × 26 cm^3, consists of an optical part, electrical circuits and a gas handling part. In the optical part, the infrared radiation was focused into the multipass cell by using two parabolic mirrors, M1 with a 10-cm reflected focal length (Thorlabs, Model MPD149-P01) and M2 with a 5-cm reflected focal length (Thorlabs, Model MPD129-P01). A chopper (Thorlabs, Model MC1F2) was placed

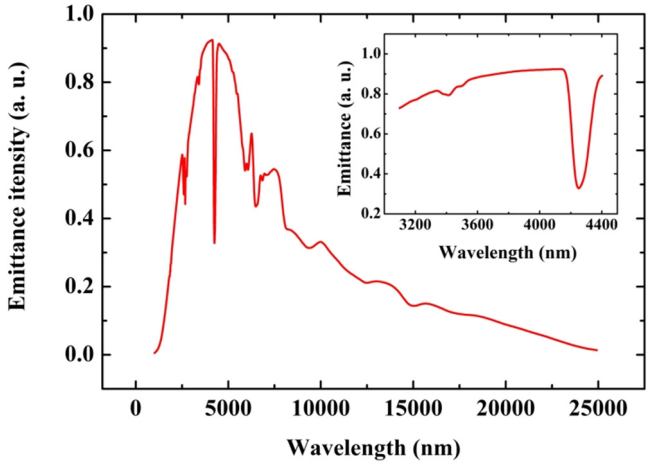

Fig. 2. Emission spectra of the broadband thermal light source in the infrared region. Inset: emission spectra in the tuning range of the FP filter from 3.1 to 4.4 μm.

between the two parabolic mirrors to modulate the light at 20 Hz, with a duty cycle of 60%. The multipass cell with a volume of 1.5 L has an optical pathlength of 2.5 m for the incoherent light beam and employs a White cell configuration, in which three spherical mirrors having the same radius of curvature are used. A White cell configuration allows for a high numerical aperture, which is beneficial to the incoherent beam coupling. The output beam from the White cell was focused on the FP filter detector employing a parabolic mirror. A 1.5-mm pinhole was placed between the parabolic mirror M3 with 5-cm reflected focal length (Thorlabs, Model MPD129-P01) and the detector in order to improve the spectral resolution by spatially filtering oblique incident beams. The tunable FP filter detector is driven by an electrical circuit board including a controllable high voltage power supply and a signal amplifier. The electronic signal from the tunable FP filter detector was amplified by the driving board and then was demodulated by a lock-in amplifier (Stanford Research Systems, USA, Model SR830) using a 12 dB/oct filter slope and 1-s time constant. The spectrum was acquired by changing the driving voltage. The waiting time between two driving voltages was set to 300 ms to allow the stabilization of the optical filter. A complete scan of the spectrum (3100–4400 nm) with a step size of 20 nm lasted ~40 s. Data collection and analysis were performed by using a LabVIEW-based software.

Certified gas samples (Beijing Air Products BAIF Gases Industry Co., LTD.) with the following concentrations were employed: pure N_2, 1% CH_4: N_2 and 0.1% CO_2:N_2, all of them with a 2% gas analytical uncertainty. A gas dilution system (Environics Inc. Model EN4000) was used to mix the gas samples at selected concentrations. A mass flow meter (Alicat Scientific, Inc. Model M-500SCCM-D) and a needle valve were placed upstream in the gas line to monitor and control the gas flow inside the cell, respectively. A gas pressure controller (MKS Instrument Inc., USA, Model 649B) was located downstream, together with a vacuum pump (KNF Technology Co., LTD, Model N813.5ANE), to maintain the pressure inside the cell at 700 Torr. Formaldehyde vapors can be added to the gas mixture by inserting a 38.5-mm diameter cylindrical diffusion cell with a liquid solution of CH_2O between the needle valve and the mass flow meter. The CH_2O vapor concentration was determined by the CH_2O liquid concentration and the flow rate of carrier gas passing through the diffusion cell. When the gas carrier flow rate was set to 100 sccm, a CH_2O vapor concentration of 0.5% was obtained.

3. Results and discussion

With an incoherent light beam, the actual number of pass counts achievable in a White cell is much less than that obtained when using

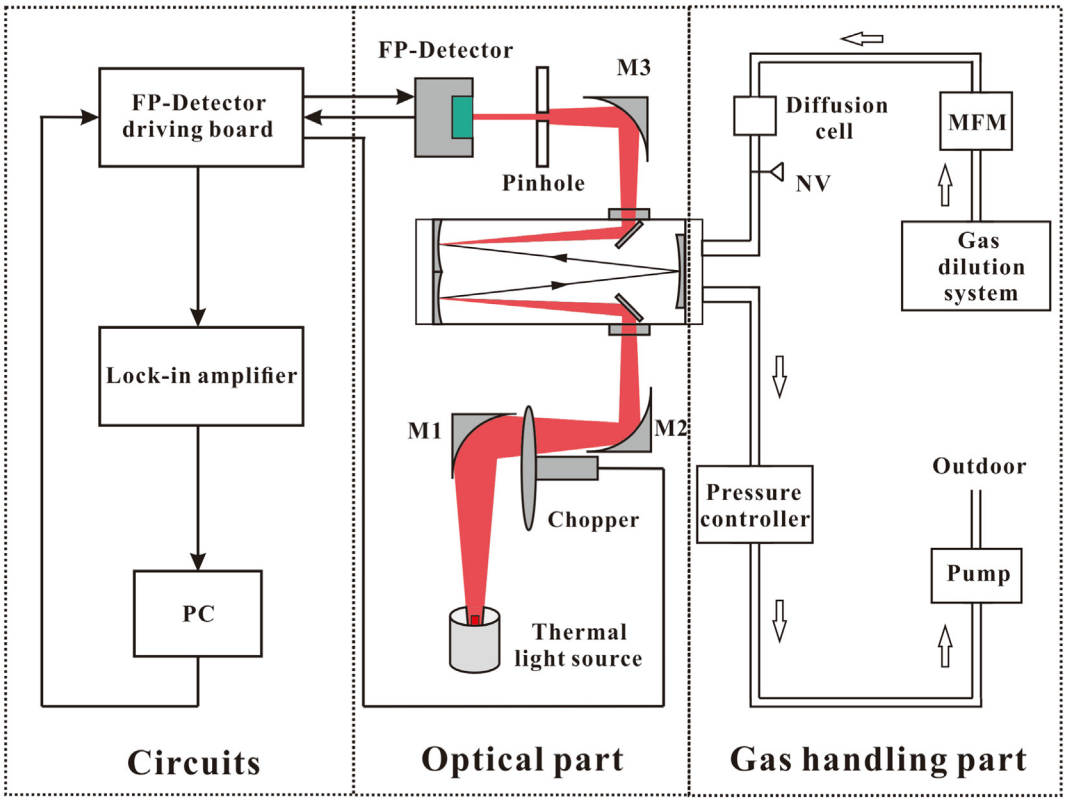

Fig. 3. Schematic of the sensor system designed for multi-gas measurements based on a tunable FP filter detector. MFM is mass flow meter; M_1, M_2, M_3 are parabolic mirrors; NV is a needle valve.

a laser beam. This is due to the much larger divergence of the incoherent beam from the thermal light source with respect to the laser beam [41]. In order to determine the effective absorption pathlength, a 0.5-m long gas cell was filled with 1% CH_4:N_2 mixture and was used as a reference. With the incoherent light beam, the 1% CH_4 spectra measured using the 0.5-m long gas cell and the White cell are shown in Fig. 4. Since the absorbance area just depends on the absorption pathlength in the case of the same target gas concentration and absorption line strength, a comparison between two areas can be used to determine the effective absorption pathlength. The ratio of the two spectral absorbance areas is ~5 times, resulting in an effective absorption pathlength of 2.5 m.

The feasibility, reliability and the validity of the sensor system was assessed by acquiring spectra of methane, formaldehyde and carbon dioxide. The spectra obtained using the multi-gas optical sensor were compared with those measured by a FTIR, as shown in Fig. 5. Pure N_2 was fed into the multipass cell to obtain the signal background in order to subtract it from the spectra acquired for different gas samples. As a result, the uneven emission spectrum of the light source and transmission window of the FP filter detector can be removed. The spectra measured for the three selected gas species using both the FTIR spectrometer and the tunable FP filter-based sensor are shown in Fig. 5. The FTIR spectrometer provides well-resolved absorption features. The FP-based multi-gas sensor well reconstructs the absorption bands of three gas species at the same wavelengths, although with a lower resolution with respect to the FTIR spectrometer.

The performance of the FP filter-based multi-gas sensor was evaluated by varying the CO_2 concentrations from 20 ppm to 1000 ppm using the gas dilution system. As shown in Fig. 6(a), the area under the absorption curve decreases while the CO_2 concentration decreases. The CO_2 concentrations as a function of absorbance area are plotted in Fig. 6(b). Each absorption spectrum was measured multiple times and the averaged values of the absorbance area was used. A polynomial fitting was implemented to calibrate the sensor system response versus CO_2 concentration. A cubic fitting of the curve with the R square value of >0.999, as shown in Fig. 6(b), yields the following expression:

$$c_{CO_2} = 8.50227 \times 10^{-8} s^3 - 1.05675 \times 10^{-5} s^2 + 5.73342 \times 10^{-4} s - 0.00742 \quad (3)$$

with s and c denoting the CO_2 spectra absorbance area and the CO_2 concentration, respectively. This expression can be used as calibration curves to retrieve the gas concentration for a single gas component in N_2.

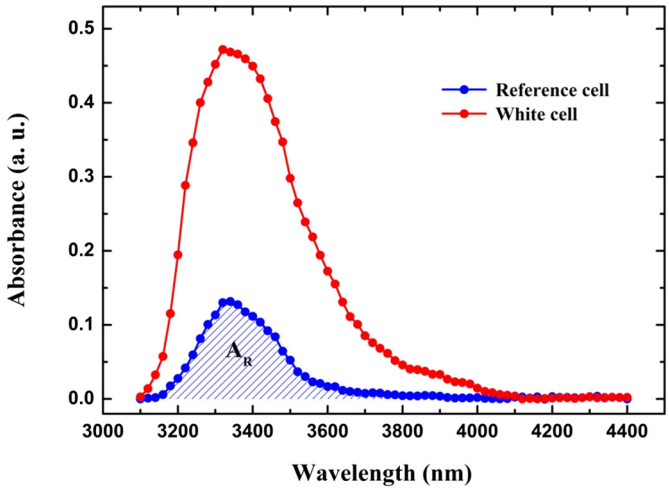

Fig. 4. 1% CH_4 absorption spectra from a reference cell (blue dot line) and a White cell (red dot line). The A_R is the absorbance area of the spectrum from the reference cell. (For interpretation of the references to colour in this figure legend, the reader is referred to the web version of this article.)

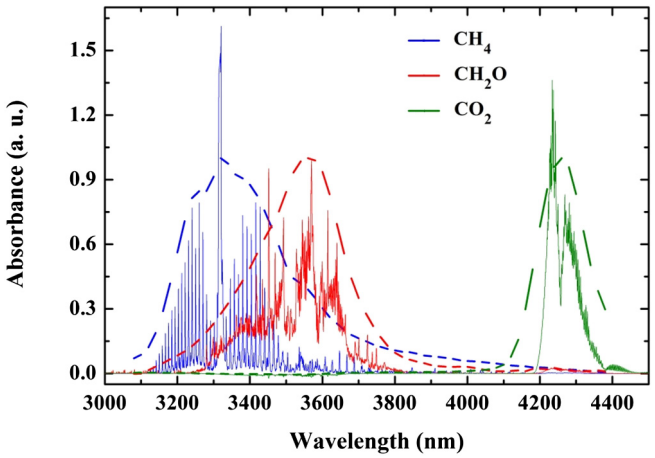

Fig. 5. Spectra of three gas samples obtained using the FTIR spectrometer (solid line) and the tunable FP filter-based sensor (dashed line). The gas species were CH_4 (blue line), CH_2O (red line) and CO_2 (green line), respectively. (For interpretation of the references to colour in this figure legend, the reader is referred to the web version of this article.)

Using the same experimental approach, the absorption spectra measured for CH_4:N_2 (with CH_4 concentration varying from 600 ppm to 10,000 ppm) and CH_2O:N_2 (with CH_2O concentration varying from 1700 ppm to 10,200 ppm) are shown in Fig. 7.

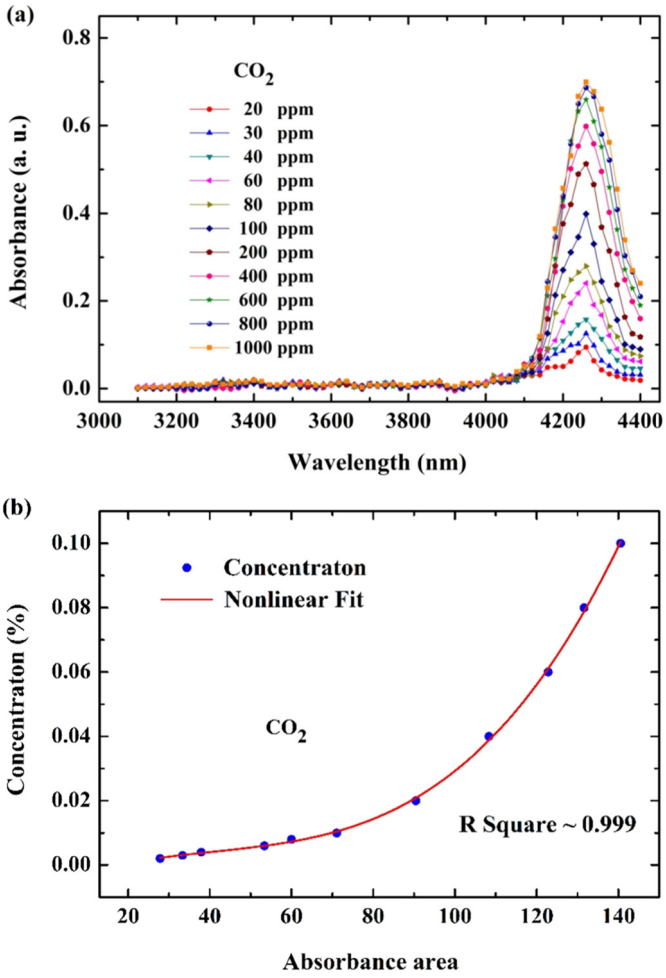

Fig. 6. (a) Absorption spectra measured for different CO_2 concentrations in N_2 in the tuning range of the FP filter-based sensor. (b) Concentration level (%) of CO_2:N_2 as a function of the absorbance area (blue dots). The red curve represents the best cubic fit of the data. (For interpretation of the references to colour in this figure legend, the reader is referred to the web version of this article.)

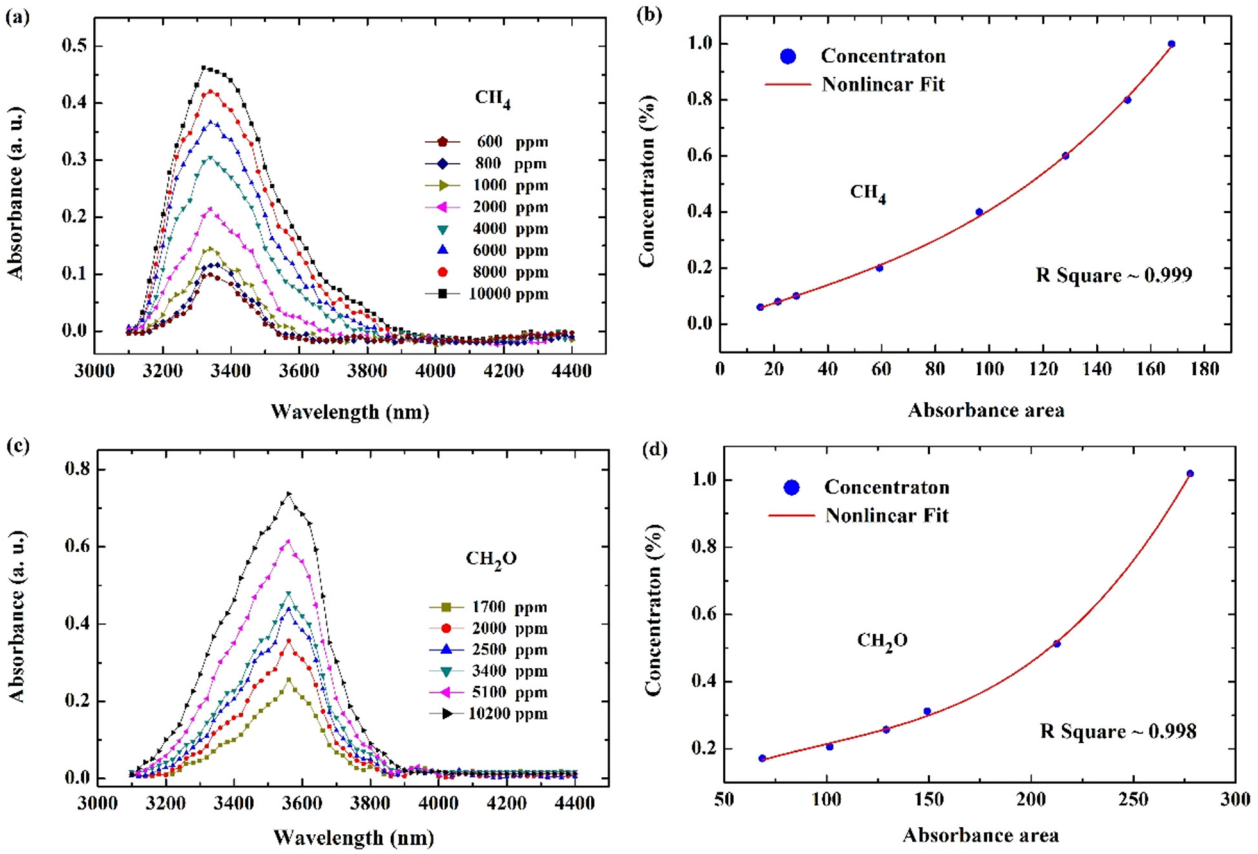

Fig. 7. Absorption spectra measured for different CH_4 (a) and CH_2O (c) concentration levels in N_2 in the tuning range of the FP filter-based sensor; Concentration levels of CH_4 (b) and CH_2O (d) as a function of the related absorbance area. The red curves represent the best cubic fits of the data. (For interpretation of the references to colour in this figure legend, the reader is referred to the web version of this article.)

The corresponding cubic best fits for CH_4:N_2 and CH_2O:N_2 are:

$$c_{CH_4} = 1.23229 \times 10^{-7}s^3 - 5.08455 \times 10^{-6}s^2 + 0.00323s + 0.01052 \quad (4)$$

and

$$c_{CH_2O} = 9.4353 \times 10^{-8}s^3 - 2.77806 \times 10^{-5}s^2 + 0.00417s - 0.01893 \quad (5)$$

The R-squared values are 0.999 and 0.998 for CH_4 and CH_2O, respectively. Detection limits of 200 ppm, 900 ppm and 20 ppm, were estimated for CH_4, CH_2O and CO_2, respectively, since their spectra could not be observed from the noise background when lower concentration levels of target gases were filled into the sensor system.

The spectral data analysis for multi-gas sensing was based on the general linear fit method. The experimentally acquired spectra were represented as a linear combination of absorption spectra of CH_4, CO_2 and CH_2O [42]:

$$S(\lambda) = \sum_{i=1}^{3} a_i S_i(\lambda) \quad (6)$$

where $S(\lambda)$ is the measured spectra as a function of the wavelength, $S_i(\lambda)$ for $i = 1$ to 3 represent the spectra of CH_4, CO_2 and CH_2O, respectively. The coefficient a_i is proportional to the concentration of the i-th compound. Once a_i values are obtained, the absorbance area for three spectra of CH_4, CO_2 and CH_2O and the related concentrations can be calculated.

The following step demonstrated the capability of the tunable FP filter-based sensor to detect multi-gas simultaneously in a single gas matrix. Initially, a mixture of 0.56% of CH_4:N_2 was sent to the diffusion cell containing the formaldehyde liquid solution using a gas flow rate of 270 sccm. Then, a 0.20% of CH_2O was added into the gas mixture by means of a diffusion effect. This gas mixture passed through the multipass gas cell. Subsequently, the mixture of 0.56% of CH_4:N_2 was replaced with a mixture of 0.04% CO_2:N_2. The CH_4 was gradually removed from the gas cell, while the CO_2 concentration level rises steadily. Due to the constant gas flow rate, the concentration level of CH_2O should remain unchanged.

Every three spectra $S(\lambda)$s were averaged to improve the detection sensitivity, resulting in a data updating rate of 2 min. The concentration evolution curves of CH_4 and CO as a function of time are shown in Fig. 8. The developed sensor was able to follow the variation of CH_4 and CO_2 concentrations versus time. The concentration levels of CH_4 decrease logarithmically with time, while the concentration levels of CO_2

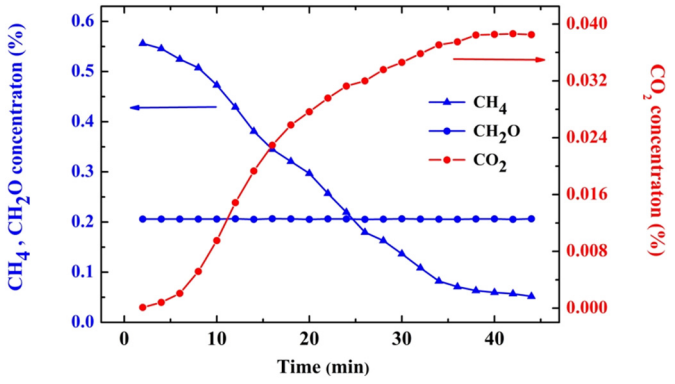

Fig. 8. Evolution of the CH_4 and CH_2O concentrations versus time. At t = 0, the CH_4:N_2 flux was stopped and CO_2:N_2 started to flow through the sensor system.

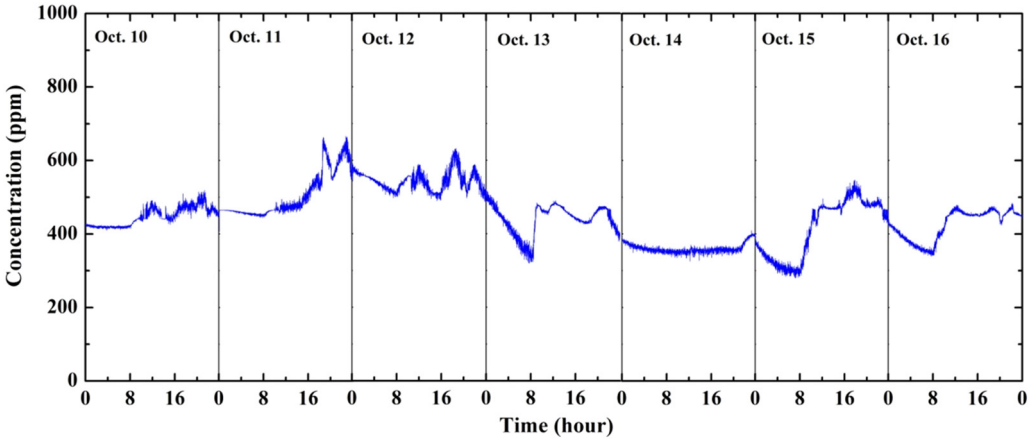

Fig. 9. CO_2 concentrations measured during a week's period in Oct. 2018 in a laboratory of the Shanxi University campus, Taiyuan, China.

increase logarithmically with time. The CH_2O concentration remains stable during all time.

4. Continuous 7-day monitoring of indoor air

A continuous 7-day monitoring of indoor air inside a laboratory located in the Shaw Amenities Building on the Shanxi University campus in Taiyuan, China, was demonstrated. The gas samples were sampled utilizing a Teflon tube with an air filter installed at the inlet to remove any dust or particulate matter. The measurements were performed at room temperature and atmospheric pressure.

The CO_2 concentration data (Oct. 10, 2018 to Oct. 16, 2018) are shown in Fig. 9. The CO_2 concentration level is closely related to staff activities. Indoor CO_2 starts to rise from 8:00 a.m. and decrease after 10:00 p.m. every day, due to the presence of staff during this time period. One exception is on Sunday, Oct. 14, 2018 since nobody entered the laboratory until 8:00 p.m. Furthermore, fluctuations of CO_2 concentration levels during workhours follow an irregular and unpredictable flow of people.

5. Conclusions

A robust, compact and cost-effective prototype of a FP filter-based sensor for real-line monitoring of a multi-gas mixture was realized and tested. To validate this system, CH_4, CH_2O and CO_2 have been used as gas targets. The spectra are well reconstructed by the FP filter-based sensor. Key components of the developed FP filter-based sensor include a broadband thermal IR light source, a tunable FP filter detector and a multipass gas cell with an effective optical path length of 2.5 m. The absorption spectra of three gas analytes at different concentrations allowed the retrieval of the related calibration curves. Detection limits of 200 ppm, 900 ppm and 20 ppm were achieved for CH_4, CH_2O and CO_2, respectively. We demonstrated the capability of the systems to perform multi-gas detection by analyzing a mixture containing CH_4, CH_2O and CO_2, using N_2 as carrier gas, and retrieving the corresponding concentrations versus time. To demonstrate the possibility to use the developed sensor system for environmental monitoring purposes, continuous monitoring of CO_2 concentration inside a laboratory-environment was carried out for one week. The measured concentration variations of CO_2 reflect the presence of people in the laboratory. The realized gas sensing system represents a cost-effective, robust and miniaturized solution that can be employed for measurement of known compositions with overlapping bands, for process control and environmental monitoring applications. It represents an interesting alternative to establish spectroscopic sensors (such as FTIR) for gas samples multi-component analysis. Further improvements in the minimum detection limit can be achieved by implementing a multipass cell with longer effective optical pathlength.

Acknowledgements

National Key Research and Development Program of China (2017YFA0304203), National Natural Science Foundation of China (NSFC) (61622503, 61575113, 61805132, 11434007), Changjiang Scholars and Innovative Research Team in University of Ministry of Education of China (IRT_17R70), 111 project (D18001), Outstanding Innovative Teams of Higher Learning Institutions of Shanxi, Foundation for Selected Young Scientists Studying Abroad, Sanjin Scholar (2017QNSJXZ-04) and Shanxi "1331KSC". Frank K. Tittel acknowledges support by the Robert Welch Foundation (Grant #C0568) The authors from Dipartimento Interateneo di Fisica di Bari acknowledge the financial support from THORLABS GmbH, within the joint-research laboratory PolySense.

References

[1] F.K. Tittel, D. Richter, A. Fried, Mid-infrared laser applications in spectroscopy, Top. Appl. Phys. 89 (2003) 445–510.
[2] P. Werle, F. Slemr, K. Maurer, R. Kormann, R. Mücke, B. Jänker, Near- and mid-infrared laser-optical sensors for gas analysis, Opt. Lasers Eng. 37 (2002) 101–114.
[3] U. Willer, M. Saraji, A. Khorsandi, P. Geiser, W. Schade, Near- and mid-infrared laser monitoringof industrial processes, environment and security applications, Opt. Lasers Eng. 44 (2006) 699–710.
[4] E.K. Shahmarvandi, M. Ghaderi, P. Ayerden, G. de Graaf, R.F. Wolffenbuttel, Implementation of CMOS-compatible metamaterial absorber for gas sensing application, Procedia Eng. 168 (2016) 1241–1244.
[5] S. Lundqvist, P. Kluczynski, R. Weih, M. von Edlinger, L. Nähle, M. Fischer, A. Bauer, S. Höfling, J. Koeth, Sensing of formaldehyde using a distributed feedback interband cascade laser emitting around 3493 nm, Appl. Opt. 51 (2012) 6009–6013.
[6] L. Dong, Y.J. Yu, C.G. Li, S. So, F.K. Tittel, Ppb-level formaldehyde detection using a CW room-temperature interband cascade laser and a miniature dense pattern multipass gas cell, Opt. Express 23 (2015) 19821–19830.
[7] G. Kraus, Infrared absorption spectroscopy of aqueous solutions with a CO_2 laser, Appl. Phys. 7 (1975) 287–293.
[8] S. Höfling, R. Weih, A. Bauer, A. Forchel, M. Kamp, Low threshold interband cascade lasers, SPIE OPTO 8631 (2013) 8631P.
[9] L. Dong, V. Spagnolo, R. Lewicki, F.K. Tittel, Ppb-level detection of nitric oxide using an external cavity quantum cascade laser based QEPAS sensor, Opt. Express 19 (2011) 24037–24045.
[10] L. Dong, R. Lewick, K. Liu, P.R. Buerki, M.J. Weida, F.K. Tittel, Ultra-sensitive carbon monoxide detection by using EC-QCL based quartz enhanced photoacoustic spectroscopy, Appl. Phys. B Lasers Opt. 107 (2012) 275–283.
[11] L. Dong, C.G. Li, N.P. Sanchez, A.K. Gluszek, R.J. Griffin, F.K. Tittel, Compact CH_4 sensor system based on a continuous-wave, low power consumption, room temperature interband cascade laser, Appl. Phys. Lett. 108 (2016), 011106. .
[12] L. Dong, F.K. Tittel, C.G. Li, N.P. Sanchez, H.P. Wu, C.T. Zheng, Y.J. Yu, A. Sampaolo, R.J. Griffin, Compact TDLAS based sensor design using interband cascade lasers for mid-IR trace gas sensing, Opt. Express 24 (2016) A528–A535.
[13] C.G. Li, L. Dong, C.T. Zheng, F.K. Tittel, Compact TDLAS based optical sensor for ppb-level ethane detection by use of a 3.34 μm room-temperature CW interband cascade laser, Sens. Actuators B Chem. 232 (2016) 188–194.

[14] D.D. Nelson, J.H. Shorter, J.B. McManus, M.S. Zahniser, Sub-part-per-billion detection of nitric oxide in air using a thermoelectrically cooled mid-infrared quantum cascade laser spectrometer, Appl. Phys. B Lasers Opt. 75 (2002) 343–350.
[15] A.A. Kosterev, R.F. Curl, F.K. Tittel, C. Gmachl, F. Capasso, D.L. Sivco, J.N. Baillargeon, A.L. Hutchinson, A.Y. Cho, Methane concentration and isotopic composition measurements with a mid-infrared quantum-cascade laser, Opt. Lett. 24 (1999) 1762–1764.
[16] B.G. Lee, M.A. Belkin, R. Audet, J. MacArthur, L. Diehl, C. Pflügl, F. Capasso, Widely tunable single-mode quantum cascade laser source for mid-infrared spectroscopy, Appl. Phys. Lett. 91 (2007), 231101. .
[17] Y.A. Bakhirkin, A.A. Kosterev, C. Roller, R.F. Curl, F.K. Tittel, Mid-infrared quantum cascade laser based off-axis integrated cavity output spectroscopy for biogenic nitric oxide detection, Appl. Opt. 43 (2004) 2257–2266.
[18] C. Chen, Q. Ren, H. Piao, P. Wang, Y.Z. Wang, A trace carbon monoxide sensor based on differential absorption spectroscopy using mid-infrared quantum Cascade laser, Micromachines 9 (2018) 670.
[19] Y. Mu, T.L. Hu, H. Gong, R.W. Ni, S.J. Li, A trace C_2H_2 sensor based on an absorption Spectrum technique using a mid-infrared Interband Cascade laser, Micromachines 9 (2018) 530.
[20] L. Lamard, D. Balslev-Harder, A. Peremans, J.C. Petersen, M. Lassen, Versatile photoacoustic spectrometer based on a mid-infrared pulsed optical parametric oscillator, Appl. Opt. 58 (2019) 250–256.
[21] M. Jahjah, W. Ren, P. Stefanski, R. Lewicki, J.W. Zhang, W.Z. Jiang, J. Tarka, F.K. Tittel, A compact QCL based methane and nitrous oxide sensor for environmental and medical applications, Analyst 139 (2014) 2065–2069.
[22] Y.C. Cao, N.P. Sanchez, W.Z. Jiang, R.J. Griffin, F. Xie, L.C. Hughes, C. Zah, F.K. Tittel, Simultaneous atmospheric nitrous oxide, methane and water vapor detection with a single continuous wave quantum cascade laser, Opt. Express 23 (2015) 2121–2132.
[23] A. Sampaolo, P. Patimisco, A. Gluszek, A. Hudzikowski, M. Giglio, H.D. Zheng, F.K. Tittel, V. Spagnolo, Low power consumption quartz-enhanced photoacoustic gas sensor employing a quantum cascade laser in pulsed operation, Int. Soc. Opt. Photonics. 10111 (2017), 101110C. .
[24] Q.X. He, C.T. Zheng, M.H. Lou, W.L. Ye, Y.D. Wang, F.K. Tittel, Dual-feedback mid-infrared cavity-enhanced absorption spectroscopy for H_2CO detection using a radio-frequency electrically-modulated interband cascade laser, Opt. Express 26 (2018) 15436–15444.
[25] F. Adler, P. Masłowski, A. Foltynowicz, K.C. Cossel, T.C. Briles, I. Hartl, J. Ye, Mid-infrared Fourier transform spectroscopy with a broadband frequency comb, Opt. Express 18 (2010) 21861–21872.
[26] J.F.D.S. Petruci, E. Tütüncü, A.A. Cardoso, B. Mizaikoff, Real-time and simultaneous monitoring of NO, NO_2, and N_2O using substrate–integrated hollow waveguides coupled to a compact Fourier transform infrared (FT-IR) spectrometer, Appl. Spectrosc. 73 (2019) 98–103.
[27] T.A. Aarhaug, A. Ferber, H. Gaertner, S. Kolås, S.O. Ryman, P. Geiser, Validation of online monitoring of PFC by QCL with FTIR spectroscopy, TMS Annual Meeting & Exhibition, Springer, Cham 2018, pp. 1487–1493.
[28] J. Workman, B. Lavine, R. Chrisman, M. Koch, Process analytical chemistry, Anal. Chem. 83 (2011) 4557–4578.
[29] D. Landgrebe, C. Haake, T. Höpfner, S. Beutel, B. Hitzmann, T. Scheper, M. Rhiel, K.F. Reardon, On-line infrared spectroscopy for bioprocess monitoring, Appl. Microbiol. Biotechnol. 88 (2010) 11–22.
[30] P.A. Wilks, In-line infrared sensors covering the mid infrared from 2 to 14 μm (5000–700 cm^{-1}), Proc. SPIE, vol. 4577, 2002, pp. 76–83.
[31] W. Luginbu, Evaluation of designed calibration samples for casein calibration in Fourier transform infrared analysis of milk, Leb. Technol. 35 (2002) 554–558.
[32] E. Vargas-Rodríguez, H.N. Rutt, Design of CO, CO_2 and CH_4 gas sensors based on correlation spectroscopy using a Fabry–Perot interferometer, Sens. Actuators B Chem. 137 (2009) 410–419.
[33] R.F. Curl, F. Capasso, C. Gmachl, A.A. Kosterev, B. McManus, R. Lewicki, M. Pusharsky, G. Wysocki, F.K. Tittel, Quantum cascade lasers in chemical physics, Chem. Phys. Lett. 487 (2010) 1–18.
[34] F.K. Tittel, R. Lewicki, R. Lascola, S. McWhorter, Emerging Infrared Laser Absorption Spectroscopic Techniques for Gas Analysis, Trace Analysis of Specialty and Electronic Gases, Wiley, Hoboken, 2013 71–110.
[35] A. Genner, C. Gasser, H. Moser, J. Ofner, J. Schreiber, B. Lendl, On-line monitoring of methanol and methyl formate in the exhaust gas of an industrial formaldehyde production plant by a mid-IR gas sensor based on tunable Fabry-Pérot filter technology, Anal. Chem. 409 (2017) 753–761.
[36] N. Neumann, M. Ebermann, K. Hiller, S. Kurth, Tunable infrared detector with integrated micromachined Fabry-Perot filter, Proc. SPIE (2007) 646606–646612.
[37] J. Antila, M. Tuohiniemi, A. Rissanen, U. Kantojärvi, M. Lahti, K. Viherkanto, M. Kaarre, J. Malinen, MEMS- and MOEMS-based near-infrared spectrometers, Encycl. Anal. Chem. (2014) 1–36.
[38] C. Gasser, A. Genner, H. Moser, J. Ofner, B. Lendl, Application of a tunable Fabry-Pérot filtometer to mid-infrared gas sensing, Sens. Actuators B Chem. 242 (2017) 9–14.
[39] M. Lacolle, I.R. Johansen, T. Bakke, H. Sagberg, Tunable diffractive filters for robust NIR and IR spectroscopy, J. Micromech. Microeng. 23 (2013), 074008. .
[40] M. Ebermann, N. Neumann, K. Hiller, E. Gittler, M. Meinig, S. Kurth, Recent advances in expanding the spectral range of MEMS Fabry-Perot filters, Proc. SPIE 7594 (2010).
[41] W. Wei, Z.H. Zhang, X.G. Hu, A white cell under the condition of non-laser, Opt. Instrum. 35 (2013) 66–70.
[42] A.A. Kosterev, P.R. Buerki, L. Dong, M. Reed, T. Day, F.K. Tittel, QEPAS detector for rapid spectral measurements, Appl. Phys. B Lasers Opt. 100 (2010) 173–180.